

Comparison of high-order harmonic generation in defect-free and defective solids with different time delays

Shujie Zhao(赵书杰), Yuanzuo Li(李源作), Jun Zhang(张军), and Xuefei Pan(潘雪飞)
Citation: Chin. Phys. B, 2025, 34 (**12**): 123201. DOI: 10.1088/1674-1056/addd82
http://cpb.iphy.ac.cn; http://iopscience.iop.org/cpb

What follows is a list of articles you may be interested in

Influence of excited states in high-order harmonic generation at intense mid-infrared field

Yan Fang(方言), Da-Wei Tian(田大纬), Yue Cao(曹玥), Xiao-Lei Hao(郝小雷), and Zheng Shu(舒正)
Chin. Phys. B, 2025, 34 (**10**): 103201. DOI: 10.1088/1674-1056/adda0d

High-order harmonic generation of methane in an elliptically polarized field

Shu-Shan Zhou(周书山), Yu-Long Li(李玉龙), Zhi-Xue Zhao(赵志学), Man Xing(幸满), Nan Xu(许楠), Hao Wang(王浩), Jun Wang(王俊), Xi Zhao(赵曦), and Mu-Hong Hu(胡木宏)
Chin. Phys. B, 2025, 34 (**6**): 063202. DOI: 10.1088/1674-1056/adcb9d

Frequency shifts of high-order harmonics from ZnO crystals by chirped laser pulses

Yu Zhao(赵宇), Xiao-Jin Liu(刘晓瑾), Shuang Wang(王爽), Xiao-Xin Huo(霍晓鑫), Yun-He Xing(邢云鹤), and Jun Zhang(张军)
Chin. Phys. B, 2025, 34 (**3**): 033201. DOI: 10.1088/1674-1056/ada9dc

Interference of harmonics emitted by different tunneling momentum channels in laser fields

Ling-Yu Zhang(张玲玉), Zhuo-Xuan Xie(谢卓璇), Can Wang(王灿), Xin-Lei Ge(葛鑫磊), and Jing Guo(郭静)
Chin. Phys. B, 2024, 33 (**9**): 093201. DOI: 10.1088/1674-1056/ad5d95

Phase-coherence dynamics of frequency-comb emission via high-order harmonic generation in few-cycle pulse trains

Chang-Tong Liang(梁畅通), Jing-Jing Zhang(张晶晶), and Peng-Cheng Li(李鹏程)
Chin. Phys. B, 2023, 32 (**3**): 033201. DOI: 10.1088/1674-1056/acac0f

---

Comparison of high-order harmonic generation in defect-free and defective solids with different time delays

Shujie Zhao(赵书杰)[1], Yuanzuo Li(李源作)[1], Jun Zhang(张军)[2], and Xuefei Pan(潘雪飞)[1,†]

[1] *College of Science, Northeast Forestry University, Harbin* 150040, *China*
[2] *Institute of Atomic and Molecular Physics, Jilin University, Changchun* 130012, *China*

(Received 3 April 2025; revised manuscript received 22 May 2025; accepted manuscript online 28 May 2025)

We theoretically investigate the high-order harmonic generation (HHG) of defect-free solids by solving the time-dependent Schrödinger equation (TDSE). The results show that the harmonic intensity can be enhanced, harmonic order can be extended, and modulation near the cutoff order becomes smaller for the second plateau by increasing the time delay. These effects are due to an increase of the electron population in higher energy bands, where the larger band gap allows electrons to release more energy, and the long electronic paths are suppressed. Additionally, we also investigate the HHG of defective solids by Bohmian trajectories (BT). It is found that the harmonic intensity of the second plateau can be further enhanced. Simultaneously, cutoff order is also extended due to Bohmian particles moving farther away from the defective zone.

Keywords: high-order harmonic generation, defective solids, Bohmian trajectories

PACS: 32.80.Rm, 42.65.Ky, 78.67.Bf

DOI: 10.1088/1674-1056/addd82 **CSTR:** 32038.14.CPB.addd82

1. Introduction

High-order harmonic generation (HHG) in the gas phase has been extensively studied over the past several decades and received widespread attention, whether in experiments or theory.[1–4] The harmonic generation has brought successful applications such as synthesizing attosecond pulses,[5,6] exploring ultrafast electron dynamics,[7,8] and imaging molecular orbitals and structures.[9,10] The experimental breakthrough of nonperturbative solid–matter harmonics in 2011 has attracted considerable attention.[11] Because the solid material has the properties of high-density electron configuration,[12,13] regular periodic structure,[14,15] natural crystal orientation,[16,17] and nonnegligible covalent bonding.[18] Therefore, the harmonic emission efficiency is higher than that of gas in the low field strength.[19] Researchers are eager to expand the success of HHG in the gases to solids.

HHG of solids originates from two different mechanisms, *i.e.*, intraband current and interband polarization.[20–22] The carriers confined to particular bands travel to perform Bloch oscillations, and intraband current arises from nonlinear optical radiation during accelerated oscillating motion.[23] A similar atomic HHG three-step model can describe the fundamental processes involved in interband polarization: the electrons tunnel from the valence band (VB) to the conduction band due to the intense laser field, then the electrons are accelerated away under the laser field. Finally the recombination of electrons with the hole leads to the emission of harmonic photons as the laser field changes direction.[24] Besides the applications of the compact-advanced light source and time-resolved dynamics, one can also measure the Berry curvature[25,26] and reconstruct band structures by utilizing HHG of solids.[27]

Recently, the time-dependent Schrödinger equation (TDSE), semiconductor Bloch equations (SBEs), and time-dependent density functional theory (TDDFT) are used to investigate the solid harmonics. The TDSE can be solved efficiently with high computational speed, yielding the time-dependent wave function and enabling the exploration of HHG in solids within multi-band systems.[28–30] SBEs in k-space accurately predict population dynamics in the highest valence band and first conduction band (CB1) and can be captured the delicate structures of the harmonic spectrum in solids.[19,22,23,31] The *ab initio* simulations of HHG in solids can be obtained by the TDDFT model, which is huge time-consuming.[32–34] We investigate the modulation properties of the second plateau of solid HHG, which involves multiple bands in this paper. The recollision model,[21,22] the strong field approximation (SFA),[35–38] and the quantitative rescattering (QRS) theory[39–41] have been generally used to illustrate the underlying physical mechanisms of HHG in solids. Besides these methods can be used to describe the motion process of electrons in solids, the electron motion can be tracked by a quantum method of Bohmian trajectories (BT).[42–48]

The Bohmian mechanics, a complementary quantum me-

†Corresponding author. E-mail: panxf@nefu.edu.cn

© 2025 Chinese Physical Society and IOP Publishing Ltd. All rights, including for text and data mining, AI training, and similar technologies, are reserved.

chanics, was first proposed by Louis de Broglie and further extended by David Bohmian, which depicts electrons as microcosmic particles in quantum phenomena.[45,47,49] Unlike the quasiclassical theoretical methods, Bohmian mechanics accurately reproduces particle trajectories of HHG and time-dependent displacement path in atoms and molecules.[45,46,50,51] It provides a clear physical picture of the complex dynamic process of atoms and molecules. It can agree well with that from numerically solving the TDSE by selecting adequate BT.[50,52,53]

The energy band can be obtained employing the Mathieu-type potential by numerically solving the TDSE, which is similar to the energy band structure of ZnO crystal.[54–57] The typical model potential has been widely used in recent investigations of the solid HHG. In order to explore the electrons motion in the defective solids, we calculate the BT. As we know, the BT can be viewed as that the wave functions guide the electronic dynamics.[58] The method of TDSE can easily calculate the wave function and have high computational speed. Therefore, the method is feasible.

As is widely recognized, the driving laser field plays an important role in HHG.[59] And recently, there has been growing interest in investigating solid-state HHG under a two-color laser field. Introducing a two-color field has been shown to benefit high-order harmonics, leading to phenomena such as two-plateau structure, enhanced harmonic intensity, modulation of HHG in ZnO crystal, and attosecond burst isolation. Li *et al*. demonstrated an intensity enhancement of the second plateau by approximately two to three orders of magnitude under an optimized two-color field.[28] Qiao *et al*. proposed an all-optical reconstruction method for three-band transition dipole moments using harmonic spectrum generated by a two-color laser field.[60] Recently, they further investigated a co-rotating two-color circularly polarized laser field and observed significant modulation of harmonic intensity in the plateau region.[61] Edwards *et al*. achieved enhanced attosecond bursts in relativistic high-order harmonics driven by two-color fields.[62] With the deepening of research on two-color laser fields, the effects of time delay between the two pulses on HHG have also been extensively studied. Feng *et al*. revealed that adjusting the time delay could optimize the harmonic spectrum, enabling the synthesis of isolated attosecond pulses without phase compensation.[63] Peng *et al*. reported HHG spectral intensity enhancement by utilizing the time delay between the two-color laser fields.[64] Frolov *et al*. demonstrated control over harmonic generation via time delay modulation.[65]

In recent theoretical studies, researchers have begun to explore the influence of defects in solids on HHG. Pattanayak *et al*. found that the total energy cutoff of the harmonic spectrum increased with higher concentration of vacancy defects, which was attributed to defects breaking the translational symmetry of the unit cell locally.[66] Additionally, Mrudul *et al*. observed that defects affected low-order harmonic generation due to defect-induced gap states.[67] Recently, Pan *et al*. demonstrated that the intensity of the second plateau of HHG could be enhanced by reducing the potential well depth of defects in solids.[51] Therefore, the distinct HHG characteristics between defect-free and defective solid-state systems under a two-color laser field with varying time delays present an intriguing domain for studying electron dynamics in condensed matter. In addition, we track the motion process of electrons by the Bohmian mechanics scheme, which introduces the concept of quantum effects of the Bohmian trajectories. The Bohmian mechanics scheme makes theoretical calculations faster and more accurate to explore the mechanism of solid-state HHG.

In this paper, we aim to explore the HHG in defect-free and defective solids induced by a two-color laser field. In defect-free solids, we find that the harmonic intensity is enhanced and the cutoff order is extended in the second plateau as the time delay increases. This is attributed to more energy being released from the second conduction band (CB2), which has a wider bandgap. Additionally, we also investigate the HHG in defective solids by analyzing the BT. The harmonic intensity of the second plateau can be further enhanced, and cutoff order is also extended because of Bohmian particles moving farther away from the defective zone.

2. Models and calculations

We theoretically investigate HHG within one dimension. In the length-gauge and dipole approximation, the TDSE can be written as[28–30] (atomic units are used throughout the paper unless otherwise specified)

$$\mathrm{i}\frac{\partial}{\partial t}\psi(x,t)=\left[\frac{1}{2}\hat{p}^2+xE(t)+V(x)\right]\psi(x,t), \tag{1}$$

where $\psi(x,t)$ and $\hat{p}$ represent the time-dependent wave function and the momentum operator. The laser field can be written as follows:

$$E(t)=E_0 f_0\cos(\omega_0 t)+E_1 f_1\cos[\omega_0(t-\tau)].$$

Here f_0 and f_1 are $\sin^2$ envelope. The duration time of the fundamental and weak laser fields are 6 and 3 optical cycles (o.c.), respectively. τ represents the the time delay between the two fields. $\omega_0=0.0154$ a.u. (atomic unit) is the frequency which corresponds to wavelength $\lambda=2957.54$ nm.

The laser filed intensity are $I_0 = 5.6 \times 10^{11}$ W/cm^2 of fundamental frequency field and $I_1 = 5.0 \times 10^{10}$ W/cm^2 of weak frequency field, respectively. $V(x) = -V_0[1 + \cos(2\pi x/a_0)]$, is the Mathieu-type potential, which satisfies the periodic condition, *i.e.*, $V(x) = V(x + a_0)$, $a_0 = 8$ a.u. is the lattice constant. In our simulation, the location of a defect in the solid is $x \in [-12$ a.u., 12 a.u.$]$.

The eigenvalue equation $H_0\phi_n(x) = E_n\phi_n(x)$ can be derived by using the finite-difference approximation method. $\phi_n(x)$ is the eigenstate wave function, where n is the eigenstate number. The operator H_0 can be written as a tridiagonal square matrix[69]

$$\begin{aligned} H_{j,j} &= \frac{1}{\Delta x^2} + V(x_j), \\ H_{j,j+1} &= -\frac{1}{2\Delta x^2}, \\ H_{j+1,j} &= H_{j,j+1}, \end{aligned} \tag{2}$$

where $V(x_j)$ is the potential of the j-th grid element and Δx is the grid space.

The time-dependent wave function can be obtained by solving second-order splitting operator method, and the harmonic spectrum can be obtained by Fourier transformation from the laser-induced current $j(t) = -\langle\psi(x,t)|\hat{p}|\psi(x,t)\rangle$

$$I(\omega) = |\int j(t)\, \mathrm{e}^{-\mathrm{i}\omega t}\, \mathrm{d}t|^2. \tag{3}$$

To illustrate the motion of electrons in solids, the trajectory of the Bohmian particles can be obtained at moment t

$$x_i(t) = x_i(t=0) + \int_0^t v_i(t')\, \mathrm{d}t', \tag{4}$$

where the velocity of Bohmian particle is

$$v_i(t) = \mathrm{Im}\left[\frac{1}{\psi_i(x,t)}\frac{\partial}{\partial t}\psi_i(x,t)|_{x=x_i(t)}\right],$$

$i = 1, 2, 3, \ldots, N_{\mathrm{tra}}$ is the number of the particle trajectories. $x_i(t=0)$ is the displacement at time $t = 0$ in the i-th trajectory.

3. Results and discussion

Figure 1(a) shows the high-order harmonic spectrum of defect-free solids induced by a two-color laser field, where the time delays are $\tau = 0$ o.c. (green dotted curve), $\tau = 1$ o.c. (red dashed curve), and $\tau = 2$ o.c. (blue solid curve), respectively. The harmonic spectrum exhibits a two-plateau structure, where the harmonic intensity of the first plateau is stronger than that of the second plateau. For the time delay $\tau = 0$ o.c., the cutoff orders for the first and second plateaus are around 24th and 82th (vertical green dashed lines). There is a large harmonic modulation in the two-plateau structure. The harmonic intensity of the second plateau is around 10^{-12} W/cm^2 (horizontal green dashed line). As the time delay increases to $\tau = 1$ o.c., the cutoff orders for the first and second plateaus are extended to around 30th and 96th (vertical red dashed lines), and the harmonic intensity is enhanced by 1 orders of magnitude compared to the time delay $\tau = 0$ o.c. in the second plateau, which the harmonic intensity is around 10^{-11} W/cm^2 (horizontal red dashed line). When the time delay increases to $\tau = 2$ o.c., the cutoff order for the first plateau is also around 30th, but the cutoff order for the second plateau is extended to around 100th (vertical blue dashed line). The harmonic intensity is enhanced by 1 order of magnitude compared to the time delay $\tau = 1$ o.c. in the second plateau, which is around 10^{-10} W/cm^2 (horizontal blue dashed line). Additionally, the harmonic modulation becomes small near the cutoff order in the second plateau. Thus, the intensity and cutoff order of high-order harmonics in defect-free solids are related to the time delay, and the harmonic modulation can be reduced by increasing the time delay.

Figure 1(b) shows the harmonic spectrum of defect-free solids with the time delay $\tau = 2$ o.c., where the weak frequency intensity is identical to those in Fig. 1(a), and the fundamental field intensity can be changed, which are $I_0 = 6.0 \times 10^{11}$ W/cm^2 (pink dotted curve), $I_0 = 7.0 \times 10^{11}$ W/cm^2 (purple dashed curve), and $I_0 = 9.0 \times 10^{11}$ W/cm^2 (brown solid curve), respectively. It is observed that the harmonic spectrum also exhibits a two-plateau structure. The harmonic intensity of the first plateau is stronger than that of the second plateau. The cutoff orders of the first plateau are both around 30th order (vertical black dashed line). There is a large harmonic modulation in the first plateau. For the fundamental field intensity $I_0 = 6.0 \times 10^{11}$ W/cm^2, the cutoff order is around 101th (vertical pink dashed line) for the second plateau. The small modulation is observed in this region. As the fundamental field intensity increases to $I_0 = 7.0 \times 10^{11}$ W/cm^2, the cutoff order for the second plateau is extended to around 104th (vertical purple dashed line). The harmonic modulation for the second plateau becomes smaller compared to the fundamental field intensity $I_0 = 6.0 \times 10^{11}$ W/cm^2, as shown in Fig. 1(b) (pink dotted curve). The harmonic intensity is enhanced compared to the fundamental field intensity $I_0 = 6.0 \times 10^{11}$ W/cm^2 in the second plateau. When the fundamental field intensity increases to $I_0 = 9.0 \times 10^{11}$ W/cm^2, the harmonic intensity in the second plateau is further enhanced compared to the fundamental field intensity $I_0 = 7.0 \times 10^{11}$ W/cm^2, as shown in Fig. 1(b) (purple dashed curve). The cutoff order of the second plateau is also extended to around 108th (vertical orange dashed line), and modulation is small in this region. Increasing the fundamental field intensity can further enhance the harmonic intensity, broaden the cutoff order, and reduce the modulation in the second plateau.

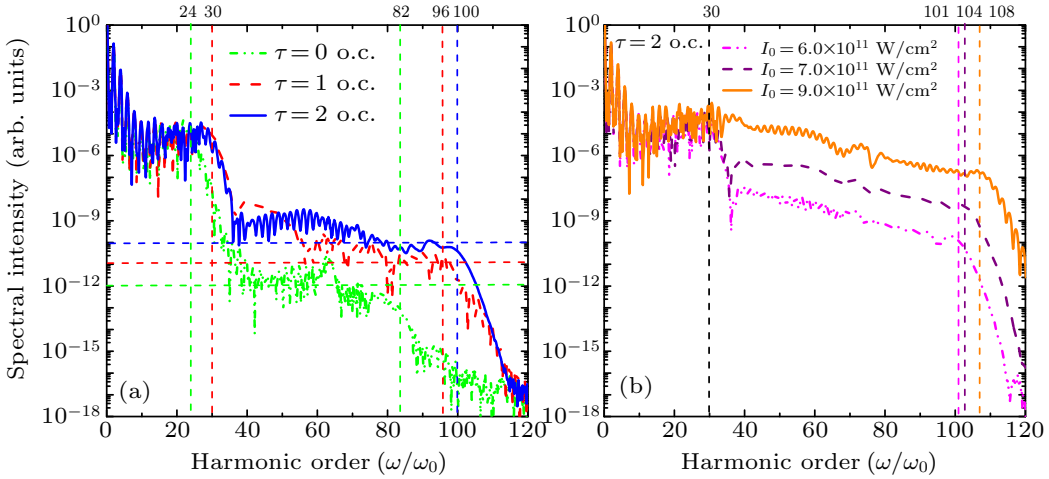


Fig. 1. The high-order harmonic spectrum of defect-free solids induced by a two-color laser field. (a) The time delays between two laser field are $\tau = 0$ o.c. (green dotted curve), $\tau = 1$ o.c. (red dashed curve), and $\tau = 2$ o.c. (blue solid curve), respectively. (b) The time delay $\tau = 2$ o.c. with the fundamental field intensity $I_0 = 6.0 \times 10^{11}$ W/cm^2 (pink dotted curve), $I_0 = 7.0 \times 10^{11}$ W/cm^2 (purple dashed curve), and $I_0 = 9.0 \times 10^{11}$ W/cm^2 (brown solid curve), respectively.

Figures 2(a1)–2(a3) illustrate the time–frequency distributions of the defect-free solid HHG induced by a two-color laser field with the time delays $\tau = 0$ o.c., $\tau = 1$ o.c., $\tau = 2$ o.c., respectively. As depicted in Fig. 2(a1), the intensity of the time–frequency distribution significantly diminishes for harmonic orders beyond the 24th. This indicates that the harmonic spectrum intensity of the second plateau is weaker compared to that of the first plateau, consistent with the harmonic spectrum shown for the time delay $\tau = 0$ o.c., as shown in Fig. 1(a) (green dotted curve). When the time delay is increased to $\tau = 1$ o.c., both long and short electronic paths are observed, as shown in Fig. 2(a2). The interference between these paths results in harmonic modulation.[68] Additionally, the intensity of the time–frequency distribution weakens for harmonic orders exceeding the 30th. Three emission peaks, labeled as A_1, A_2, and A_3, are observed. The emission peak A_2 exhibits the strongest intensity and plays a dominant role in the harmonic generation of the second plateau. When the time delay is further increased to $\tau = 2$ o.c., it is observed that the three emission peaks shift to right, labeled as B_1, B_2, and B_3, and emission peaks B_2 and B_3 exhibit the significant intensity, which play the dominant role in the harmonic generation of the second plateau. The intensity of the time–frequency distribution is enhanced compared to the case with the time delay $\tau = 1$ o.c., as shown in Fig. 2(a3). Only the short electronic paths is observed, the interference between the long and short electronic paths will reduce, and it results in small harmonic modulation, which is consistent with the harmonic spectrum for the time delay $\tau = 2$ o.c., as shown in Fig. 1(a) (blue solid curve). These findings indicate that the intensity of the harmonics in the second plateau can be enhanced by increasing the time delay, and harmonic modulation is reduced due to the suppression of long electronic paths.

Figures 2(b1)–2(b3) illustrate the time–frequency distribution of the defect-free solid HHG spectrum induced by a two-color laser field. Keeping the time delay of two-color laser field constant at $\tau = 2$ o.c., the fundamental field intensity is set to $I_0 = 6.0 \times 10^{11}$ W/cm^2, $I_0 = 7.0 \times 10^{11}$ W/cm^2, and $I_0 = 9.0 \times 10^{11}$ W/cm^2, respectively. As depicted in Fig. 2(b1), three emission peaks, labeled as C_1, C_2, and C_3, are observed. The emission peak C_2 has the strongest intensity among them, which plays a dominant role in the harmonic generation for the second plateau. The long electronic paths are suppressed. When the fundamental field intensity is increased to $I_0 = 7.0 \times 10^{11}$ W/cm^2, the intensity of the three emission peaks, labeled as D_1, D_2, and D_3, is significantly enhanced compared to the case with the fundamental field intensity $I_0 = 6.0 \times 10^{11}$ W/cm^2. Additionally, the intensity of short electronic paths is enhanced, whereas long electronic paths remain suppressed. The interference between the long and short electronic paths will further reduce, and the harmonic spectrum will become smooth. These results are consistent with second plateau of harmonic spectrum, as shown in Fig. 1(b). When the fundamental field intensity is further increased to $I_0 = 9.0 \times 10^{11}$ W/cm^2, the intensity of three emission peaks, labeled as E_1, E_2, and E_3, is enhanced, and the strongest emission peak E_2 plays a dominant role in the harmonic generation for the second plateau. The short electronic paths are further enhanced. When the time delay is fixed at $\tau = 2$ o.c., the intensity of time–frequency distribution of harmonic spectrum above 30th order is enhanced, and the short electronic paths are enhanced, whereas the long electronic paths remain suppressed, as the fundamental field intensity increases. This further explains that increasing the fundamental field intensity can enhance the intensity of the time–frequency distribution of HHG spectrum, and suppress the long electronic paths, ultimately enhancing the harmonic intensity and reducing the harmonic modulation of the second plateau, as shown in Fig. 1(b).

To explore the physical mechanism of the harmonic intensity enhancement, we also investigate the electron population

of the defect-free solids. Figures 3(a1)–3(a3) show the population of the CB1 induced by a two-color laser field with the time delays $\tau = 0$ o.c., $\tau = 1$ o.c., $\tau = 2$ o.c., respectively. Figures 3(b1)–3(b3) show the corresponding population of the CB2. For the population of the CB1, it is observed that emission peaks appear every half optical cycle. The electron population is around the order of magnitude 10^{-4} . However, the population in the CB2 is 3 or 4 orders of magnitude lower than that in CB1. Due to the wider bandgap, the electrons in CB2 can release more energy than those in CB1 when they return and recombine with holes in the VB.[28,60] The more energy extends the cutoff order. However, the harmonic intensity of the first plateau is significantly stronger than that of the second plateau, due to the more population of electrons in CB1 compared to CB2, as shown in Fig. 1(a).

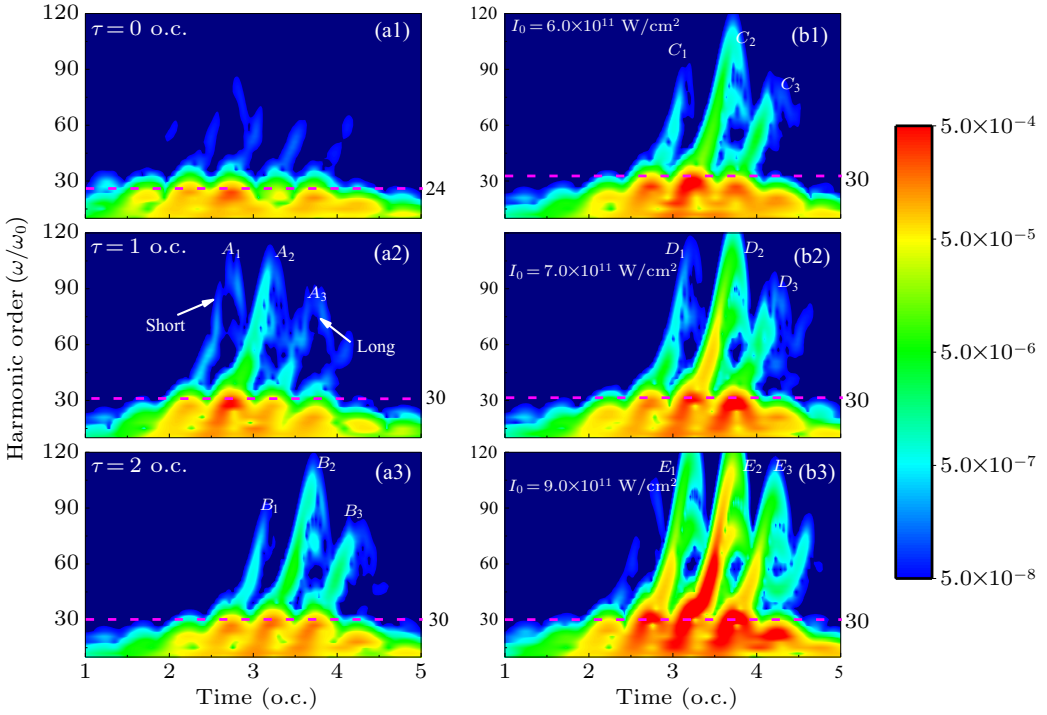


Fig. 2. The time–frequency distribution of the defect-free solid HHG spectrum induced by a two-color laser field. The time delays between two laser field are (a1) $\tau = 0$ o.c., (a2) $\tau = 1$ o.c., and (a3) $\tau = 2$ o.c., respectively. Keeping the time delay of two-color laser field constant at $\tau = 2$ o.c., the fundamental field intensity is set to (b1) $I_0 = 6.0 \times 10^{11}$ W/cm^2, (b2) $I_0 = 7.0 \times 10^{11}$ W/cm^2, and (b3) $I_0 = 9.0 \times 10^{11}$ W/cm^2, respectively.

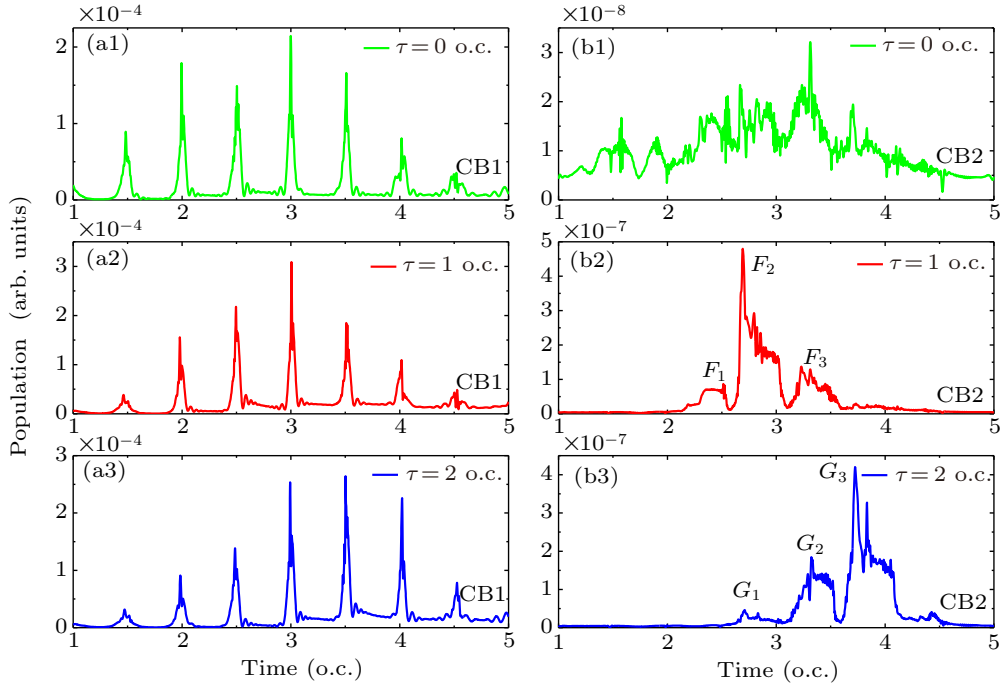


Fig. 3. The time-dependent electron population of the defect-free solids. (a1)–(a3) Electron population of CB1, and (b1)–(b3) the corresponding electron population of CB2, the time delay (a1) and (b1) $\tau = 0$ o.c., (a2) and (b2) $\tau = 1$ o.c., and (a3) and (b3) $\tau = 2$ o.c.

As depicted in Fig. 3(b1), the electron population is around the order of magnitude 10^{-8} and exhibits irregular emission peaks. When the time delay is increased to $\tau = 1$ o.c., as shown in Fig. 3(b2), the electron population is 1 orders of magnitude more than that for the time delay $\tau = 0$ o.c., as shown in Fig. 3(b1). The more electrons there are, the more energy is released when they recombine with holes, and thus the stronger the harmonic intensity becomes. This indicates that harmonic intensity of the second plateau is enhanced at the time delay $\tau = 1$ o.c. compared to the case with the time delay $\tau = 0$ o.c., as shown in Fig. 1(a) (green dotted curve and red dashed curve). Three emission peaks, labeled as F_1, F_2, and F_3, are observed. The emission peak F_2 has the strongest intensity, which plays a dominant role in the harmonic generation for the second plateau. The number of emission peaks in Fig. 3(b2) is identical to that in Fig. 2(a2), and the strongest emission peaks A_2 and F_2 are at the middle position. These indicate that the population in CB2 influences the intensity of the time–frequency distribution of HHG spectrum. When the time delay is further increased to $\tau = 2$ o.c., it is observed that the three emission peaks, labeled as G_1, G_2, and G_3, shift to right, and emission peaks G_2 and G_3 play a dominant role in the harmonic generation for the second plateau. The number of emission peaks in Fig. 3(b3) is identical to that in Fig. 2(a3), and the emission peaks B_2, B_3 and G_2, G_3 are at the middle and rear positions. These provide further evidence that the population in CB2 influences the intensity of the time–frequency distribution of the HHG spectrum.

We also investigate the high-order harmonic spectrum of defective solids. The potential energy curve for the defective solids are shown in Fig. 4(a). The red solid curve represents the defective solids, with a potential well depth of $V_0 = 0.37$ a.u. The defect is located at $x \in [-12$ a.u., 12 a.u.$]$. Figure 4(b) shows the the high-order harmonic spectrum induced by a two-color laser field with the time delays $\tau = 0$ o.c. (green dotted curve), $\tau = 1$ o.c. (red dashed curve), and $\tau = 2$ o.c. (blue solid curve), respectively. The harmonic spectrum also exhibits a two-plateau structure. For the time delay $\tau = 0$ o.c., the cutoff orders of the first and second plateaus are around 22th and 78th (vertical green dashed lines), respectively. The harmonic intensity of the second plateau is around 10^{-9} W/cm^2 (horizontal green dashed line), which is significantly enhanced by 3 orders of magnitude compared to the case of defect-free for the time delay $\tau = 0$ o.c. as shown in Fig. 1(a) (green dotted curve). When the time delay is increased to $\tau = 1$ o.c., the cutoff orders are extended to 30th and 92th (vertical red dashed lines), respectively. The harmonic intensity of the second plateau is around 10^{-8} W/cm^2 (horizontal red dashed line), which is enhanced compared to that for the time delay $\tau = 0$ o.c., as shown in Fig. 4(b) (green dotted curve). Furthermore, it is enhanced by 3 order of magnitude compared to the case of defect-free for the time delay $\tau = 1$ o.c., as shown in Fig. 1(a) (red dashed curve). The harmonic intensity of the second plateau is around 10^{-7} W/cm^2 (horizontal blue dashed line), which is enhanced by 3 orders of magnitude compared to the case of defect-free for the time delay $\tau = 2$ o.c., as shown in Fig. 1(a) (blue solid curve).

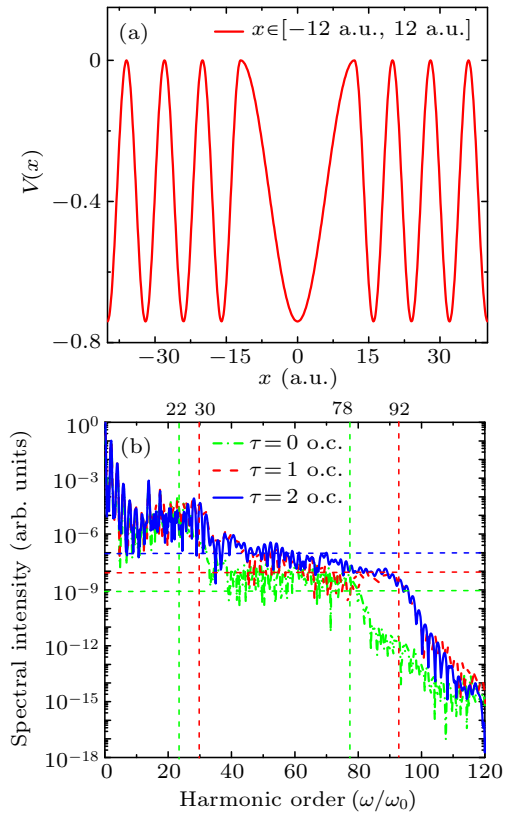


Fig. 4. The potential energy curve and the high-order harmonic spectrum of defective solids. (a) The red solid curve represents the defective solids. (b) The high-order harmonic spectrum of defective solids are induced by a two-color laser field with the time delays $\tau = 0$ o.c. (green dotted curve), $\tau = 1$ o.c. (red dashed curve), and $\tau = 2$ o.c. (blue solid curve), respectively. Other parameters of laser field are identical to those in Fig. 1(a).

To explore the physical mechanisms of defective harmonic spectrum, we investigate the time–frequency distribution of HHG spectrum and BT in defective solids. Figures 5(a1)–3(a3) show the time–frequency distributions of HHG induced by a two-color laser field with the time delays $\tau = 0$ o.c., $\tau = 1$ o.c., $\tau = 2$ o.c., respectively. As depicted in Fig. 5(a1), five emission peaks are observed, where the starting time of the strongest emission peak, labeled as H, is around 2.4 o.c., which plays a dominant role in the harmonic generation. It is also observed that the intensity of the emission peaks is enhanced compared to the case with the time delay $\tau = 0$ o.c., as shown in Fig. 2(a1). This indicates that the harmonic intensity of the second plateau from defective solid is stronger than that from the defect-free solids. When the time delay is increased to $\tau = 1$ o.c., as shown in Fig. 5(a2), the five emission peaks are observed, and the intensity of the emission peaks is enhanced compared to the case with the time

delay $\tau = 0$ o.c., as shown in Fig. 5(a1). The starting time of the strongest emission peak, labeled as J, is around 2.9 o.c. which is right-shifted compared to the case with the time delay $\tau = 0$ o.c., as shown in Fig. 5(a1). When the time delay further increases to $\tau = 2$ o.c., the intensity of the emission peaks is enhanced, and the strongest emission peak, labeled as K, is further right-shifted. The starting time of the emission peak K is around 3.4 o.c. These confirm that the harmonic intensity of the second plateau in defective solids is stronger than that in defect-free solids under the same conditions, and it can be further enhanced by increasing the time delay.

Figures 5(b1)–5(b3) show the BT of defective solids induced by a two-color laser field with the time delays $\tau = 0$ o.c., $\tau = 1$ o.c., $\tau = 2$ o.c., respectively. It is observed that the evolution of the BT can be divided into two kinds. The first kind of particles are always located in the defective zone of solids ($x \in [-12$ a.u., 12 a.u.$]$). The second kind of particles move away from the defective zone to the negative direction. Specifically, the emission time of harmonic spectrum of solids from the time–frequency distribution agrees well with the time that the BT change direction.[51] The farther the particles move, the more energy they carry. When the laser field reverses, the recombination of electrons and holes emits high-order harmonics with a broader range of orders. As depicted in Figs. 5(a1) and 5(b1), the starting time of the strongest emission peak H aligns with the time of the direction change in BT, which is around 2.4 o.c., as indicated by the vertical pink dashed line. Meanwhile, the position of Bohmian particles of the direction change in the BT is around 25 a.u. (cyan solid arrow). When the time delay is increased to $\tau = 1$ o.c., the position of Bohmian particles of the direction change in the BT is turned into around 50 a.u. (cyan solid arrow) at the time of 2.9 o.c, at which the starting time of the strongest emission peak J aligns with the time of Bohmian particles of the direction change in BT, which is indicated by the vertical pink dashed line, as shown in Figs. 5(a2) and 5(b2). This explains the extension of the cutoff order in the second plateau, which is due to Bohmian particles moving farther away from the defective zone for the time delay $\tau = 1$ o.c. compared to the case for the time delay $\tau = 0$ o.c. When the time delay is further increased to $\tau = 2$ o.c., the position of Bohmian particles of the direction change in the BT remains around 50 a.u. (cyan solid arrow) at the time of 3.4 o.c, which is indicated by the vertical pink dashed line, as shown in Figs. 5(a3) and 5(b3). This further confirms that the cutoff order in the second plateau is determined by Bohmian particles moving farther away from the defective zone, as shown in Figs. 5(b2) and 5(b3).

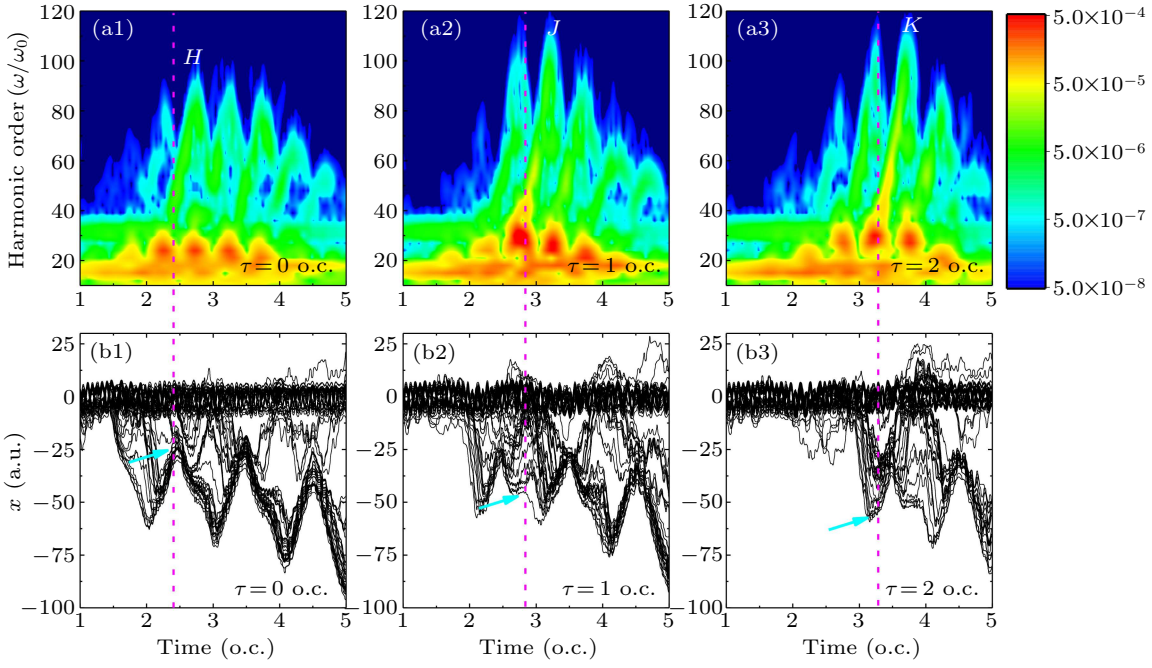


Fig. 5. The time–frequency distribution of the HHG spectrum and BT of defective solids. (a1)–(a3) The time–frequency distribution of the HHG spectrum, and (b1)–(b3) the corresponding BT, the time delay (a1) and (b1) $\tau = 0$ o.c., (a2) and (b2) $\tau = 1$ o.c., and (a3) and (b3) $\tau = 2$ o.c.

To better illustrate the influence of different types and locations of defective solids on harmonic spectra, we investigate HHG in defective solids with potential well depths of $V_0 = 0$ a.u. (red dashed curve), $V_0 = 0.26$ a.u. (blue dotted curve), and $V_0 = 0.52$ a.u. (pink short-dotted curve), as shown in Fig. 6(a1). The location of the the potential wells is at $x \in [-12$ a.u., 12 a.u.$]$. For comparisons, the black solid curve represents defect-free solids with a potential well depth of $V_0 = 0.37$ a.u. The corresponding harmonic spectra are shown in Fig. 6(a2). It can be observed that the first plateau is significantly extended (pink dashed vertical line) for potential well depths of $V_0 = 0$ a.u. and $V_0 = 0.26$ a.u., whereas the

second plateau becomes narrower (cyan solid vertical line). In contrast, for $V_0 = 0.52$ a.u., the harmonic spectrum inelarly matches that of defect-free solids. These results indicate that the depth of the defective potential well significantly affects HHG, with deeper potential well exhibiting weaker influence.

We also calculate the HHG spectra for different defective locations. The locations are at $x \in [-36$ a.u., -12 a.u.] (red dashed curve), $x \in [36$ a.u., 60 a.u.] (blue dotted curve), as shown in Fig. 6(b1). The potential well depth is $V_0 = 0.37$ a.u., and the black solid curve represents defect-free solids. The corresponding harmonic spectra are shown in Fig. 6(b2). It can be observed that the firs plateau is significantly extended (pink dashed vertical line), while the second plateau completely disappears. Additionally, the harmonic intensity is remarkably enhanced compared to that of defect-free case. By comparing the harmonic spectra in Figs. 6(a2) and 6(b2), we can conclude that both potential well depth and defective locations can significantly alter the structural characteristics of the harmonic spectra. Specifically, the defective locations can lead to the complete disappearance of the second plateau.

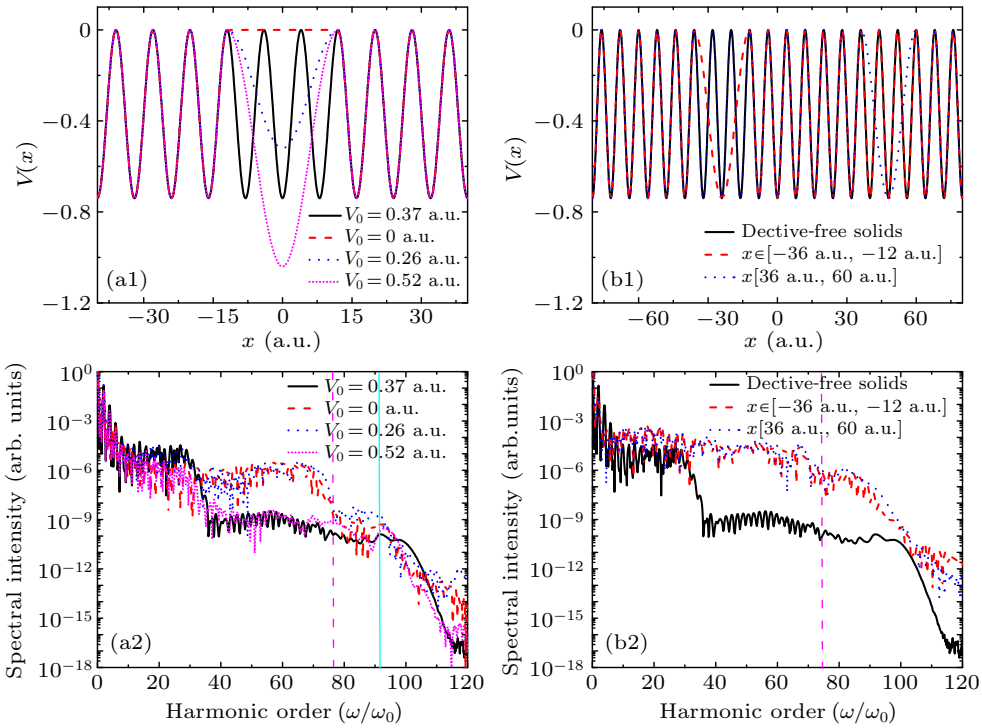


Fig. 6. The potential well depths, the defective locations, and the corresponding harmonic spectra. (a1) The potential well depths are $V_0 = 0$ a.u. (red dashed curve), $V_0 = 0.26$ a.u. (blue dotted curve), $V_0 = 0.52$ a.u. (pink short-dotted curve). The black solid curve represents defect-free solids with a potential well depth $V_0 = 0.37$ a.u. (a2) The corresponding harmonic spectra for the cases shown in panel (a1). (b1) The defective locations are at $x \in [-36$ a.u., -12 a.u.] (red dashed curve) and $x \in [36$ a.u., 60 a.u.] (blue dotted curve). The black solid curve represents a defect-free solids. (b2) The corresponding harmonic spectra for the cases shown in panel (b1).

4. Conclusion

To sum up, we investigate the HHG of defect-free and defective solids induced by a two-color laser field with the time delays $\tau = 0$ o.c., $\tau = 1$ o.c., $\tau = 2$ o.c., respectively. It can be observed that the harmonic intensity of defect-free solids is enhanced, and the cutoff order is extended for the second plateau by increasing the time delay. This is because more energy can be released when electrons transition from the CB2 to the VB. Additionally, the modulation near the cutoff order can be reduced in the second plateau due to the suppression of the long electronic paths as the time delay increases. We also investigate the HHG of defective solids and find that the harmonic intensity in the second plateau is further enhanced compared to that of defect-free solids. Besides, cutoff order is also extended due to Bohmian particles moving farther away from the defective zone. Further investigations can explore different potential well depths and the locations of defect sites in solids. Additionally, the effects of nonlinear laser fields or different solid materials (such as MgO, SiO_2, ZnS, *etc.*) on the HHG can be studied. Moreover, all the above researches directions can be extended to two-dimensional systems. These studies will advance the understanding of HHG in defective solids.

Acknowledgements

Project supported by the Natural Science Foundation of Jilin Province of China (Grant No. 20230101014JC), the Fundamental Research Funds for the Central Universities (Grant No. 2572021BC05), and the National Natural Science Foundation of China (Grant No. 12374265).

References

[1] Corkum P B 1993 *Phys. Rev. Lett.* **71** 1994

[2] Smirnova O, Mairesse Y, Patchkovskii S, Dudovich N, Villeneuve D, Corkum P and Ivanov M Y 2009 *Nature* **460** 972

[3] Zhang J, Ge X L, Wang T, Xu T T, Guo J and Liu X S 2015 *Phys. Rev. A* **92** 013418

[4] Huo X X, Wang S, Sun L, Xing Y H, Zhang J and Liu X S 2022 *Phys. Rev. A* **106** 023102

[5] Sola I J, Mével E, Elouga L, Constant E, Strelkov V, Poletto L, Villoresi P, Benedetti E, Caumes J P, Stagira S, Vozzi C, Sansone G and Nisoli M 2006 *Nat. Phys.* **2** 319

[6] Zhao K, Zhang Q, Chini M, Wu Y, Wang X W and Chang Z H 2012 *Opt. Lett.* **37** 3891

[7] Corkum P B and Krausz F 2007 *Nat. Phys.* **3** 381

[8] Géneaux R, Kaplan C J, Yue L, ROSS A D, Bækhhøj J E, Kraus P M, Chang H T, Guggenmos A, Huang M Y, Zürch M, Schafer K J, Neumark D M, Gaarde M B and Leone R 2007 *Nat. Phys.* **3** 381

[9] Woźniak A P and Moszyński R 2024 *Phys. Rev. A* **109** 013523

[10] Li L, Lan P F, He L X, Cao W, Zhang Q B and Lu P X 2020 *Phys. Rev. Lett.* **124** 157403

[11] Ghimire S, Dichiara A D, Sistrunk E, Agostini P, Dimauro L F and Reis A 2011 *Nat. Phys.* **7** 138

[12] You Y S, Reis D A and Ghimire S 2017 *Nat. Phys.* **13** 345

[13] Ndabashimiye G, Ghimire S, Wu M, Browne D A, Schafer K J, Gaarde M B and Reis D A 2016 *Nature* **534** 520

[14] Li L, Lan P F, Zhu X S, Huang T F, Zhang Q B, Lein and Lu P X 2019 *Phys. Rev. Lett.* **122** 193901

[15] Wang Y, Shao T J, Li X F, Liu Y, Jiang P Z, Zhang W, Zhang L F, Bian X B, Liu Y Q, Gong Q H and Wu C Y 2023 *Opt. Lett.* **31** 3379

[16] Song X H, Yang S D, Zuo R X, Meier T and Yang W F 2020 *Phys. Rev. A* **101** 033410

[17] He Y L, Guo J, Gao F Y and Liu X S 2022 *Phys. Rev. B* **105** 024305

[18] Jiménez-galán Á, Bossaer C, Ernotte G, Parks A M, Silva R E F, Villeneuve D M, Staudte A, Brabec T, Luican-mayer A and Vampa G 2022 *Nat. Commun.* **14** 8421

[19] Huttner U, Kira M and Koch S W 2017 *Laser Photon. Rev.* **105** 1700049

[20] Kruchinin S Y, Krausz F and Yakovlev V S 2018 *Rev. Mod. Phys.* **90** 021102

[21] Higuchi T, Stockman M I and Hommelhoff P 2014 *Phys. Rev. Lett.* **113** 213901

[22] Mcdonald C R, Vampa G, Corkum P B and Brabec T 2015 *Phys. Rev. A* **92** 033845

[23] Vampa G, Mcdonald C R, Orlando G, Klug D D, Corkum P B and Brabec T 2014 *Phys. Rev. Lett.* **113** 073901

[24] Vampa G, Hammond T J, Thiré N, SchmidT B E, Légaré F, Mcdonald C R, Brabec T and Corkum P B 2015 *Nature* **522** 462

[25] Liu H Z, Li Y L, You Y S, Ghimire S, Heinz T F and Reis D A 2017 *Nat. Phys.* **13** 262

[26] Luu T T and Wörner H J 2018 *Nat. Commun.* **9** 916

[27] Borsch M, Schmid C P, Weigl L, Schlauderer S, Hofmann N, Lange C, Steiner J T, Kock S W, Huber R and Kire M 2020 *Science* **370** 1204

[28] Li J B, Zhang X, Yue S J, Wu H M, Hu B T and Du H C 2017 *Opt. Express* **25** 18603

[29] Jin J Z, Xiao X R, Liang H, Wang M X, Chen S G, Gong Q H and Peng L Y 2018 *Phys. Rev. A* **97** 043420

[30] Mrudul M S, Pattanayak A, Ivanov M and Dixit G 2019 *Phys. Rev. A* **100** 043420

[31] Zhao Y T, Ma S Y, Jiang S C, Yang Y J, Zhao X and Chen J G 2019 *Opt. Express* **27** 34392

[32] Tancogne-dejean N, Mücke O D, Kärtner F X and Rubio A 2017 *Nat. Commun.* **8** 745

[33] Tancogne-dejean N, Mücke O D, Kärtner F X and Rubio A 2017 *Phys. Rev. Lett.* **118** 087403

[34] Floss I, Lemell C, Wachter G, Smejkal V, Sato S A, Tong X M, Yabana K and Burgdörfer J 2018 *Phys. Rev. A* **97** 011401

[35] Lewenstein M, Balcou P, Ivanov M Y, L'huillier A and Corkum P B 1994 *Phys. Rev. A* **49** 2117

[36] L'huillier A, Lewenstein M, Salières P and Balcou P 1993 *Phys. Rev. A* **48** R3433

[37] Amini K, Biegert J, Calegari F, Chacón A, Ciappina M F, Dauphin A, Efimov D K, Figueira De morisson faria C, Giergiel K, Gniewek P, Landsman A S, Lesiuk M, Mandrysz M, Maxwell A S, Moszyński R, Ortmann L, Antonio Pérez-hernández J, Picón A, Pisanty E, Prauzner-bechcicki J, Sacha K, Suárez N, Zaïr A, Zakrzewski J and Lewenstein M 2019 *Rep. Progr. Phys.* **82** 116001

[38] Qiao Y, Wang N, Jiang S C, Yang Y J, Chen G J and Dorfman K 2024 *Phys. Rev. B* **110** 075201

[39] Hoang V H and Le A T 2020 *Phys. Rev. A* **102** 023112

[40] Han J X, Guan Z, Wang B Y and Jin C 2023 *Chin. Phys. B* **12** 124210

[41] Qiao Y, Huo Y Q, Liang H Q, Chen J G, Liu W J, Yang Y J and Jiang S C 2023 *Phys. Rev. B* **107** 075201

[42] Song Y, Guo F M, Li S Y, Chen J G, Zeng S L and Yang Y J 2012 *Phys. Rev. A* **86** 033424

[43] Huang Y Y, Lai X Y and Liu X J 2018 *Chin. Phys. B* **27** 073204

[44] Li D D, Duan J Q, Lin L and Zhang A 2021 *Chaos* **31** 101101

[45] Lai X Y and Liu X J 2020 *Chin. Phys. B* **29** 013205

[46] Pan X F, Li B, Qi T, Zhang J and Liu X S 2021 *Phys. B: At. Mol. Opt. Phys.* **54** 025601

[47] Song S M, Wu L Y, Qiao Y, Zhou S S, Wang J, Guo F M and Yang Y J 2023 *Symmetry* **15** 581

[48] Song Y, Han S, Yang Y J and Guo F M 2024 *Chin. Phys. B* **33** 123201

[49] Jooya h Z, Telnov D A, Li P C and Chu S H 2015 *Phys. Rev. A* **91** 063412

[50] Song Y, Guo F M, Li S Y, Chen J G, Zeng S L and Yang Y J 2012 *Phys. Rev. A* **86** 033424

[51] Pan X F, Mu H B, Qi D W, Zhang J and Liu X S 2022 *Europhys. Lett.* **138** 45001

[52] Peatross J and Johansen J 2014 *Opt. Express* **22** 576

[53] Xu L and He F 2019 *J. Opt. Soc. Am. B* **36** 840

[54] Guan Z, Zhou X X and Bian X B 2016 *Phys. Rev. A* **93** 033852

[55] Liu Z, Zhao J, Dong W P, Liu J L, Huang Y D and Zhao Z X 2017 *Phys. Rev. A* **96** 053403

[56] Du T Y, Guan Z, Zhou X X and Bian X B 2016 *Phys. Rev. A* **94** 023419

[57] Jia G R, Wang X Q, Du T Y, Huang X H and Bian X B 2018 *J. Chem. Phys.* **149** 154308

[58] Pan X F, Li B, Zhang J and Liu X S 2021 *J. Phys. B: At. Mol. Opt. Phys.* **54** 025601

[59] Chen J Q, Jiang W L, Qiao Y, Yang Y J and Chen J G 2025 *Chin. Phys. Lett.* **42** 013201

[60] Qiao Y, Huo Y Q, Jiang S C, Yang Y J and Chen J G 2022 *Opt. Express* **30** 9971

[61] Qiao Y, Chen J Q, Zhou S S, Chen J G, Jiang S C and Yang Y J 2024 *Chin. Phys. Lett.* **41** 014205

[62] Edwards M R, Platonenko V T and Mikhailova J M 2014 *Opt. Lett.* **24** 6823

[63] Feng L Q and Chu T S 2012 *J. Electron Spectrosc. Relat. Phenom.* **185** 39

[64] Peng D, Pi L W, Frolov M V and Starace A F 2017 *Phys. Rev. A* **95** 033413

[65] Frolov M V, Manakov N L, Minina A A, Vvedenskii N V and Slilaev A A 2018 *Phys. Rev. Lett.* **120** 263203

[66] Pattanayak A, Mrudul M S and Dixit G 2020 *Phys. Rev. A* **101** 013404

[67] Mrudul M S, Tancogne-dejean N, Rubio A and Dixit G 2020 *npj Comput. Mater.* **6** 6617

[68] Ge X L, Du H, Wang Q, Guo J and Liu X S 2015 *Chin. Phys. B* **24** 023201s

[69] Liu X, Zhu X S, Lan P F, Zhang X F, Wang D, Zhang Q B and Lu P X 2017 *Phys. Rev. A* **95** 063419